RESEARCH ARTICLE | JANUARY 12 2026

Epitaxial configuration of unidirectionally aligned MoS_2 monolayer on sapphire

Akihiro Ohtake ; Jun Nara ; Yoshiki Sakuma

J. Appl. Phys. 139, 024303 (2026)
https://doi.org/10.1063/5.0303598

Journal of Applied Physics ARTICLE pubs.aip.org/aip/jap

Epitaxial configuration of unidirectionally aligned MoS_2 monolayer on sapphire

Cite as: J. Appl. Phys. **139**, 024303 (2026); doi: 10.1063/5.0303598
Submitted: 23 September 2025 · Accepted: 17 December 2025 ·
Published Online: 12 January 2026

Akihiro Ohtake,[a] Jun Nara, and Yoshiki Sakuma

AFFILIATIONS

National Institute for Materials Science (NIMS), Tsukuba 305-0044, Japan

[a]**Author to whom correspondence should be addressed:** OHTAKE.Akihiro@nims.go.jp

ABSTRACT

Highly oriented MoS_2 monolayer (ML) on the sapphire(0001) substrate was grown by metal-organic chemical vapor deposition. The epitaxial configuration of ML-MoS_2/sapphire has been studied using low-energy electron diffraction (LEED) combined with first-principles calculations. LEED analysis based on the dynamical diffraction theory revealed that the MoS_2 ML is grown with the epitaxial relationship of MoS_2 [$11\bar{2}0$] // Al_2O_3 [$11\bar{2}0$] and MoS_2 [$1\bar{1}00$] // Al_2O_3 [$1\bar{1}00$] and that the formation of antiparallel (inversion) domains is effectively suppressed. The observed epitaxial relationship is insensitive to the direction of surface steps on the sapphire substrate.

I. INTRODUCTION

Monolayer (ML) transition-metal dichalcogenides (TMDCs) have attracted considerable research interest, because of their unique electrical and optical properties. In particular, ML-MoS_2 has been considered one of the most promising 2D materials for substantial potential applications in electronic and optoelectronic devices. The synthesis of ML-MoS_2 on sapphire, scalable and industry-compatible substrates, is crucial from an industrial perspective and is suitable for a wide range of advanced electronic and optoelectronic applications, particularly those requiring transparency and excellent electrical insulation.

Numerous studies have reported the successful epitaxial growth of wafer-scale MoS_2 ML on the sapphire substrate using a variety of growth methods such as powder-source chemical vapor deposition (CVD)[1–7] and metal-organic CVD (MOCVD).[8–11] However, the epitaxial ML-MoS_2 film on sapphire substrates often contains both parallel (0°, 120°, or 240° domain) [Fig. 1(a)] and antiparallel (60°, 180°, or 300° domain) [Fig. 1(b)] domains.[1,2,6,8] The coexistence of inverted domains potentially induces optical scattering and reduces carrier mobilities at domain boundaries, which severely degrade the electrical and optoelectronic properties of the MoS_2 film. Thus, unidirectional alignment of MoS_2 on sapphire is highly preferred for achieving high-quality, wafer-scale single-crystalline films that are essential for advanced electronic and optoelectronic applications.

Several attempts have been made recently to realize unidirectional alignment of MoS_2 on sapphire.[3–5,7,9,11] Determination of the epitaxial relationship is crucial to confirm whether the unidirectional alignment is achieved. Epitaxial relationship between MoS_2 and sapphire has extensively studied using a variety of experimental techniques such as optical microscopy,[1–3,5–7] atomic-force microscopy,[4,9] x-ray diffraction (XRD),[6,8–10] electron diffraction,[3–5,8,11] and cross-sectional transmission electron microscopy (TEM).[3–5,7,11] Epitaxially grown MoS_2 islands often exhibit triangular shapes and show preferential alignment of their edges along certain crystallographic directions of the sapphire substrate. While such macroscopic alignment could be observed in optical microscopy and atomic-force microscopy images, it is usually not sufficient to conclusively determine the precise epitaxial orientation. In addition, the orientation of MoS_2 triangular islands enclosed by Mo-terminated edges is rotated by 180° with respect to those with S-terminated edges,[12] which makes it difficult to determine whether the ML-MoS_2 films were grown on the sapphire substrate in a parallel or antiparallel configurations.

Cross-sectional TEM directly provides information about atomic structures at the MoS_2/Al_2O_3 interface,[3–5,7,11] which enables us to clearly distinguish parallel and antiparallel configurations. However, TEM data may not be fully representative of the whole sample, because atomic structures in a localized area are imaged in TEM. While XRD has been widely used to study the

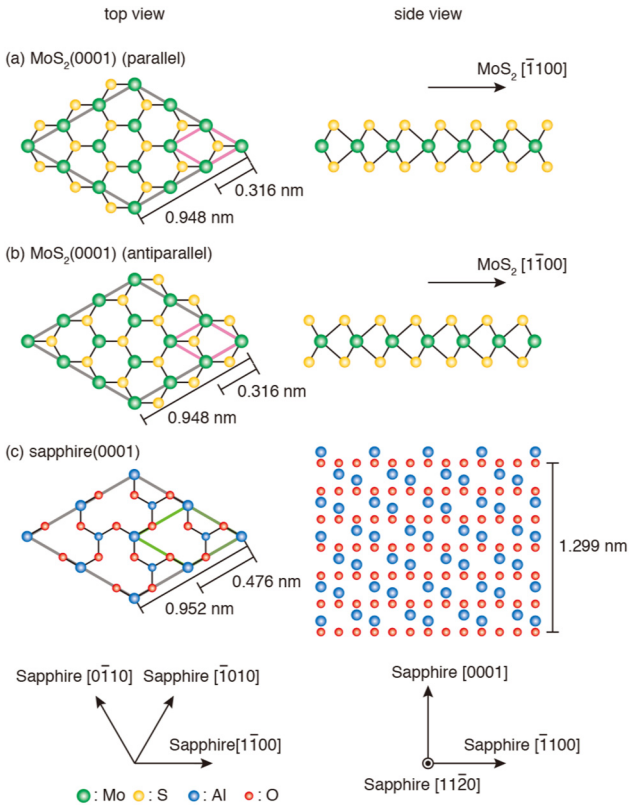

FIG. 1. Schematic drawings of MoS_2(0001) [(a) and (b)] and Al_2O_3(0001) (c) lattices. The MoS_2 lattices in (a) and (b) are in parallel and antiparallel configurations, respectively, with the Al_2O_3 lattice.

epitaxial relationship between MoS_2 and sapphire,[6,8–11] parallel and antiparallel configurations could not be distinguished by conventional XRD measurements.

This paper reports a combined experimental and theoretical study on the detailed epitaxial orientation of ML-MoS_2 on the c-plane sapphire substrate. From low-energy electron diffraction (LEED) analysis based on dynamical diffraction theory, we found that the MoS_2 ML on sapphire is unidirectionally aligned in the parallel configuration, i.e., $[1\bar{1}00]MoS_2$ // $[1\bar{1}00]$sapphire [Figs. 1(a) and 1(c)] over the whole sample. Theoretical calculations revealed that the stability of unidirectionally oriented MoS_2 ML critically depends on the atomic registry between the MoS_2 and the sapphire lattices.

II. EXPERIMENTAL

The samples were prepared using the MOCVD reactor.[11] The 2 in. c-sapphire substrates with a miscut angle of −0.2° along the m-axis direction (c/m = −0.2°) were procured by Orbray Co. Ltd. and were cut into 20 × 20 mm^2 pieces for the growth experiments. Prior to the growth, the substrates were annealed in a muffle furnace at 1150 °C for 1 h to produce a step-and-terrace structure with ML-height steps. The ML-MoS_2 film was grown at a substrate temperature of 975 °C using molybdenum oxychloride (MoO_2Cl_2) and hydrogen sulfide (H_2S) as the molybdenum and sulfur precursors, respectively. The complete surface coverage was attained by 60 min. The uniformity of the MoS_2 coverage was confirmed by Raman and AFM measurements.[11] Representative AFM images and Raman spectra were shown in Figs. S1 and S2, respectively, in the supplementary material.

The samples were analyzed by LEED (OCI BDL600IR) under ultrahigh vacuum (UHV) conditions at 1×10^{-8} Pa. Before the LEED measurements, the samples were degassed at 150 °C for 30 min in UHV. The LEED patterns were acquired at room temperature with a 1 eV step in the energy range of 30–380 eV. The LEED intensity–voltage (I–V) curves for five nonequivalent beams were extracted from LEED patterns with the background being subtracted. The total cumulative energy range (ΔE) was approximately 1455 eV. The samples were also characterized by reflection high-energy electron diffraction (RHEED) (Staib EK-35-R) with an electron beam energy of 20 keV.

III. CALCULATIONS

Theoretical calculations were performed by using the PHASE/0 code,[13] which is based on DFT[14] and pseudo-potential schemes[15,16] with plane-wave basis sets. For the exchange-correlation term, the PBE form was used.[17] For the van der Waals interactions, the DFT-D2 method was applied.[18] The cutoff energies for the wavefunctions and charge density were 56 and 506 Ry, respectively. The number of k points sampled in the Brillouin zone was more than 5 × 5 per the surface unit cell of c-plane sapphire. All the models were optimized to meet the force criterion of 0.02 eV/Å. Sapphire slab employed here consists of six Al_2O_3 layers and the thickness of a vacuum region is 0.9 nm. The top (bottom) layer of a sapphire slab is terminated with only one Al atom per surface unit, to make its electronic states semiconducting. The calculated lattice constant for the hexagonal MoS_2 monolayer is 0.318 nm, while that for sapphire is 0.4798 nm. In this study, the change in the lattice mismatch of MoS_2 grown on sapphire is quite essential to see the stability of MoS_2/sapphire heterostructures. Thus, the lattice constant for sapphire is set to 0.4789 nm to follow the experimental ratio of 1.506 for MoS_2 and sapphire. This treatment is justified, because there is no chemical bond between MoS_2 monolayer and sapphire slab, and the lattice constant of sapphire slab is not affected by MoS_2. Adsorption energy, E_{ad} is defined as $E_{ad} = (E^{MoS_2} + E^{sapphire} - E^{MoS_2/sapphire})/S$, where E^{MoS_2}, $E^{sapphire}$, and $E^{MoS_2/sapphire}$ are the calculated total energies for MoS_2 monolayer, sapphire, and MoS_2/sapphire, respectively. S is the area of a superstructure. In this definition, the larger E_{ad} is, the more stable the system is.

IV. RESULTS AND DISCUSSION

Figures 2(a) and 2(b) show RHEED patterns of the sapphire (0001) substrate taken from the $[11\bar{2}0]$ and $[\bar{1}100]$ directions, respectively. The asymmetric features of the RHEED pattern observed along the $[11\bar{2}0]$ direction indicate the threefold symmetry of the sapphire (0001) surface, which is more clearly seen in LEED patterns [Fig. 2(d)], in which the intensity of the 1 0 spot is

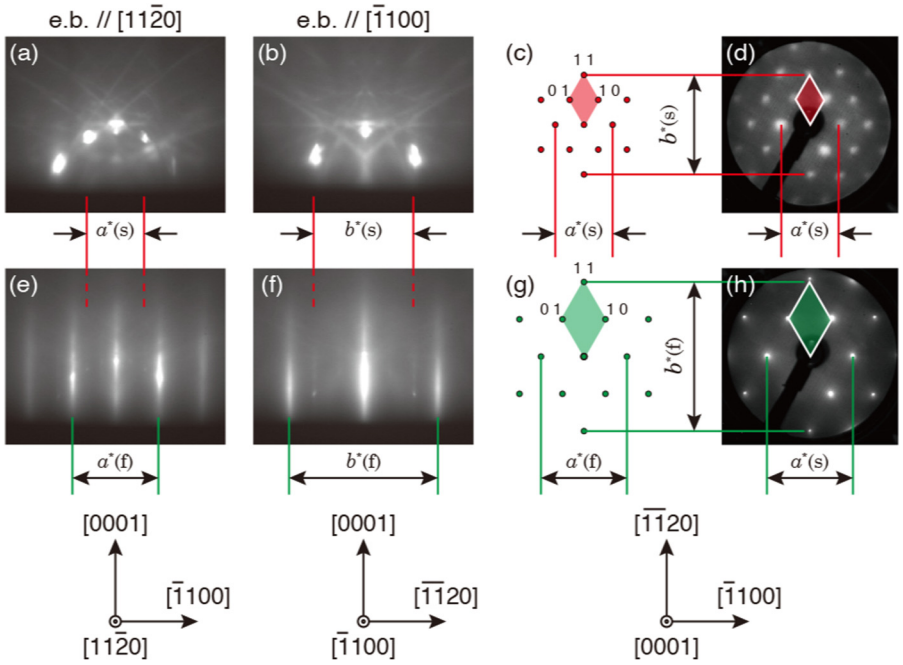

FIG. 2. RHEED patterns of the sapphire(0001) substrate (a) and (b) and 1 ML-MoS_2(0001) (e) and (f) taken along the [11$\bar{2}$0] and [$\bar{1}$100] directions of sapphire. (c) and (g) show schematic drawing of reciprocal lattices of sapphire and MoS_2, respectively. LEED patterns taken from sapphire (d) and MoS_2 (h) with an incident electron beam energy of 120 eV.

higher than that of the 0 1 spot. The RHEED patterns of 1 ML-MoS_2 film grown on the sapphire substrate are shown in Figs. 2(e) and 2(f). The spacings of streaks [$a^*(f)$ and $b^*(f)$ in Figs. 2(e) and 2(f)] are 1.5 times larger than those of sapphire [$a^*(s)$ and $b^*(s)$ in Figs. 2(a) and 2(b)] in both [11$\bar{2}$0] and [$\bar{1}$100] directions, being consistent with lattice constants of sapphire (0.476 nm) and MoS_2 (0.316 nm). Thus, it turns out that the crystalline MoS_2(0001) films were grown on the sapphire(0001) substrate with the epitaxial relationship of MoS_2 [1$\bar{1}$00] // sapphire [1$\bar{1}$00]. However, from the results in Fig. 2, it is difficult to determine if [1$\bar{1}$00] directions of MoS_2 and sapphire are in a parallel [Fig. 1(a)] or antiparallel [Fig. 1(b)] configuration with the sapphire substrate [Fig. 1(c)].

Figures 3(a)–3(c) show LEED patterns of 1 ML-MoS_2 taken from the three locations across the sample. It is clearly seen that the spot intensities in LEED patterns measured at all of the locations drastically change with the incident electron beam energy: whereas LEED patterns taken at 190 and 240 eV show threefold symmetry, the relative intensities of spots A and B are reversed. In contrast, a sixfold symmetry is observed at 204 eV. We confirmed that almost identical LEED patterns were observed at eight measurement points on the sample.

To identify whether the ML-MoS_2 films were grown on the sapphire substrate in a parallel or antiparallel configuration, we performed LEED I–V curve analysis on the basis of dynamical diffraction theory. LEED I–V curves were calculated using SATLEED package provided by Barbieri and Van Hove.[19,20] The present calculation used 10 phase shifts for the description of the electron-crystal interaction. The inner potential $V_0 + iV_{im}$ was set to be independent of energy: the real part V_0 was initially set to be 10 eV and adjusted during the fitting process and the imaginary part V_{im} was set to be −4 eV. The isotropic thermal vibrational amplitudes represented by Debye temperatures were also optimized to obtain good agreement with the experimental I–V curves. The resultant Debye temperatures are 800 K for both Mo and S atoms. To quantify the agreement between measured and calculated I–V curves, we use Pendry's reliability factor (R_P).[21]

Figure 3(d) shows measured LEED I–V curves together with the calculated ones from the MoS_2 ML. This calculations assumed that the ML-MoS_2(0001) lattice is perfectly aligned to the sapphire (0001) lattice with the epitaxial relationship of MoS_2 [1$\bar{1}$00] // sapphire [1$\bar{1}$00], as shown in Figs. 1(a) and 1(c) (parallel configuration). As a first step of the analysis, for simplicity, I–V curves were calculated from the isolated ML-MoS_2(0001)-(1×1) model using atomic coordinates fixed at bulk values. The analysis yields the overall R factor of R_P = 0.29, showing a good agreement with the LEED experiments: as indicated by vertical dashed lines in Fig. 3(d), the intensity of the 1 0 (0 1) spot is higher than that of the 0 1 (1 0) spot at 190 eV (240 eV) for both measured and calculated I–V curves. On the other hand, as shown in Fig. 4(c), when the antiparallel configuration [Figs. 1(b) and 1(c)] was considered, the calculation could not reproduce the experimental I–V curves (R_P = 1.00), suggesting that the formation of antiparallel domains (inversion domains) could be effectively suppressed. These results clearly show that LEED spots A, B, C, D, and E could be indexed as 1 0, 0 1, 1 1, 2 0, and 0 2 reflections, respectively, and that the MoS_2 grows on the sapphire substrate with its [1$\bar{1}$00] direction parallel to the sapphire [1$\bar{1}$00] direction (parallel configuration). In addition, when I–V curves were calculated for bilayer MoS_2 [Fig. 4(d)] and bulk MoS_2 [Fig. 4(e)], they resulted in larger R factors (R_P = 0.47 for 2 ML-MoS_2 and 0.48 for bulk MoS_2),

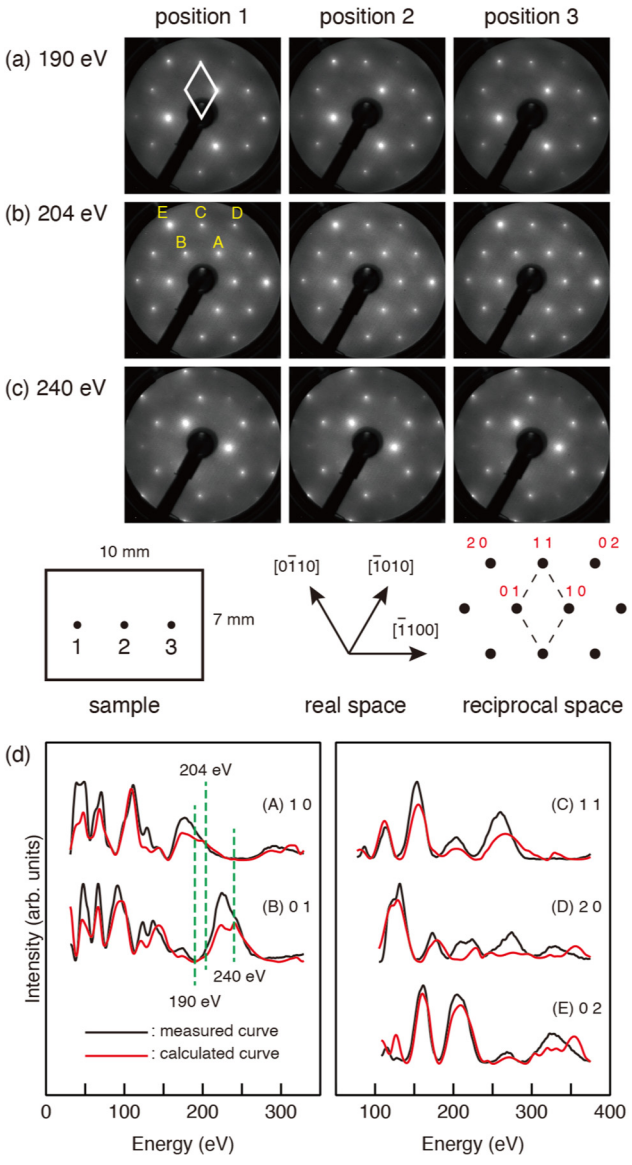

FIG. 3. LEED patterns taken from three locations across the 1 ML-MoS_2/sapphire sample with incident electron beam energies of 190 (a), 204 (b), and 240 eV (c). (d) Measured (red) and calculated (blue) LEED *I–V* curves.

indicating that the MoS_2 film mainly consists of ML-MoS_2 domains. This is in good agreement with AFM observations.[11]

Since, as mentioned earlier, the in-plane lattice constant of sapphire is approximately 1.5 times larger than that of MoS_2, the MoS_2 (3 × 3) supercell aligned in the same direction of the Al_2O_3 (2 × 2) cell reduces the effective lattice mismatch from −33.6% to −0.42%. Possible atomic configurations of MoS_2 (3 × 3)/Al_2O_3 (2 × 2) superstructure are shown in Figs. 5(a)–5(c). In the models A and C, as indicated with dashed circles, Mo and S atoms are located just above the surface Al atoms, respectively, whereas surface Al atoms are located beneath the center of Mo-S hexagon in the model B. To study the relative stability of these models, we performed theoretical calculations. The present calculations assumed the Al_2O_3 surface terminated with a single Al layer [Fig. 5(d)], which has been reported most energetically stable[22,23] and has been confirmed by experiments.[24,25] After the structural optimization, the surface Al atoms in models A and B are displaced downward by a large amount of 0.07–0.08 nm from their initial position (horizontal dashed line). On the other hand, in the model C, a slight upward displacement (∼0.02 nm) is observed. The atomic displacements of Mo and S atoms from their positions in optimized ML-MoS_2 are much less than 0.01 nm in all models.

The energetic stability of MoS_2/sapphire strongly depends on the lateral registry between MoS_2 and Al_2O_3 lattices: the models A and B have 61 meV and 66 meV higher adsorption energies per (3 × 3) unit cell, respectively, than the model C. We performed LEED analysis using the optimized atomic coordinates for MoS_2 (3 × 3)/Al_2O_3 (2 × 2) superstructures. As compared with the analysis using unrelaxed MoS_2(1 × 1) model (R_P = 0.29), the models A and B show improved *R* factors of R_P = 0.24 and R_P = 0.23, respectively, whereas no significant improvement was found for the model C (R_P = 0.28). The statistical error limit, $var(R) = R_{min}\sqrt{(8V_{im}/\Delta E)}$,[21] was estimated to be 0.034, indicating a significant difference between models A and B and model C. Thus, we conclude that the models A and B are more likely for the MoS_2/Al_2O_3 interface structure.

The present experiments show that the epitaxial orientation of MoS_2 on sapphire is uniquely determined with the MoS_2 [11$\bar{2}$0] and [1$\bar{1}$00] directions being aligned with the Al_2O_3 [11$\bar{2}$0] and [1$\bar{1}$00] directions, respectively (parallel configuration). On the other hand, our DFT calculations show that the difference in the adsorption energy between the parallel and antiparallel domains is negligibly small (energy difference ≈ 0.1 meV/MoS_2(1 × 1)).[11] Thus, the present experimental results could not be explained by the energetic stability. Another possible explanation for the onset of the parallel configuration is based on the presence of surface steps on the sapphire substrates. Early studies have shown that the presence of step edges on the substrate enables the unidirectional alignment of MoS_2 domains:[3] triangular MoS_2 islands are nucleated with their edges being parallel to the surface steps on the sapphire substrate, thus facilitating the unidirectional alignment of MoS_2 domains. Specifically, the use of sapphire substrate with the miscut orientation towards the [11$\bar{2}$0] axis promotes the unidirectional alignment of 90°-rotated MoS_2 domains on sapphire.[3]

To study whether surface steps play a crucial role in determining the epitaxial orientation, we prepared sapphire substrates with different miscut orientations, as shown in Fig. 6(a). The miscut directions and angles of the sapphire substrate were evaluated by XRD rocking-curve measurements (see Fig. S3 in the supplementary material). Figure 6(b) compares LEED *I–V* curves measured from the ML-MoS_2 grown on the three substrates; almost identical results were obtained irrespective of the direction of steps on the sapphire substrate. All of the measured curves (A-C) are in good agreement with the calculated ones for the MoS_2/sapphire models shown in Figs. 5(a) and 5(b); R_P is in the range of 0.22∼0.24. These results clearly show that the direction of surface

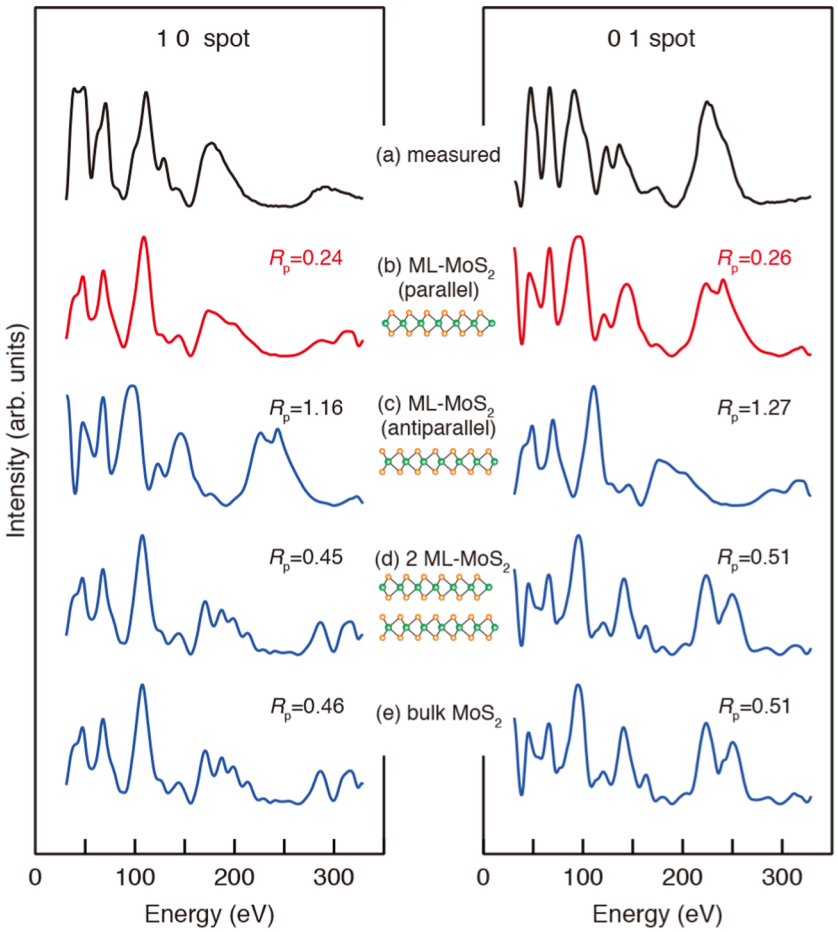

FIG. 4. (a) LEED *I–V* curves measured from the 1 ML-MoS_2 sample. Calculated *I–V* curves for 1 ML-MoS_2 on sapphire in parallel (b) and antiparallel (c) configurations. Curves (d) and (e) were calculated from 2 ML MoS_2 and bulk MoS_2, respectively.

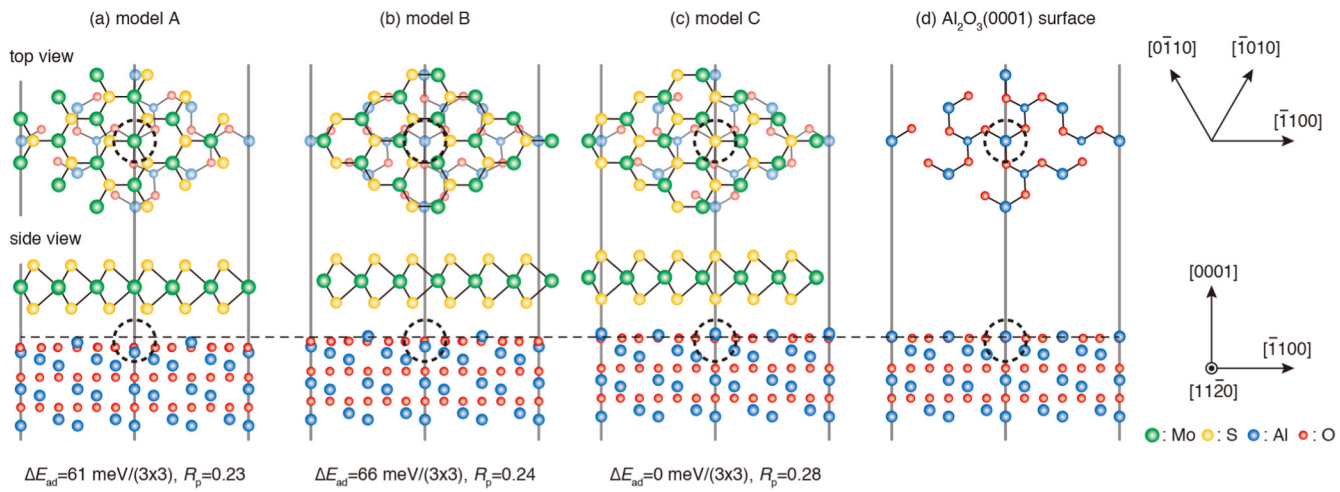

FIG. 5. Schematics of $MoS_2(3 \times 3)/Al_2O_3(2 \times 2)$ superstructures with different lateral registries between MoS_2 and Al_2O_3 (a–c) and the Al_2O_3 surface (d). Horizontal dashed line indicates the vertical position of the surface Al atom of the Al_2O_3 substrate in (d).

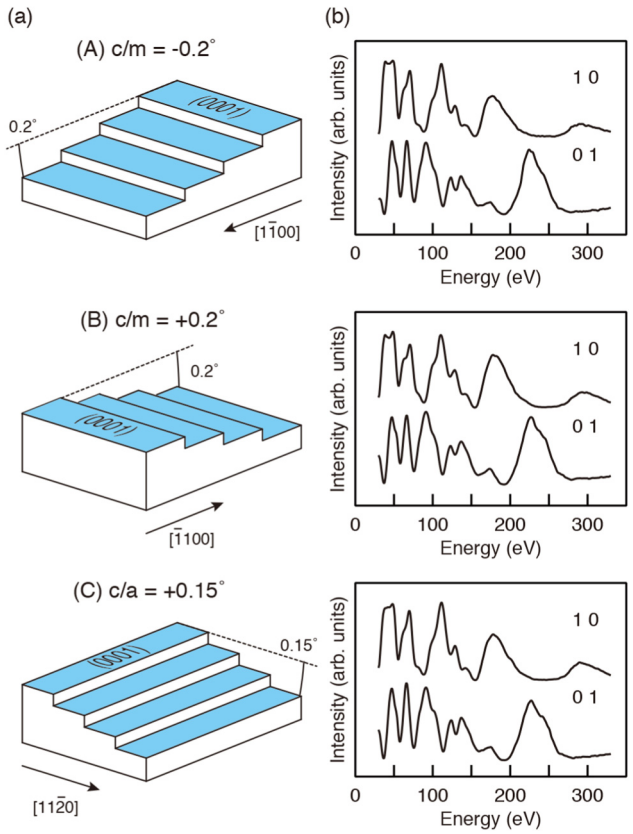

FIG. 6. (a) Schematic illustrations of sapphire substrates with miscut angles of ~0.2° along the [1$\bar{1}$00] (A), [$\bar{1}$100] (B), and [11$\bar{2}$0] (C) directions. The miscut angles determined by the XRD measurements are c/m = −0.2485° (A), c/m = +0.199° (B), and c/a = +0.1586° (C). (b) LEED *I*–*V* curves of ML-MoS_2 grown on sapphire substrates with different off-directions.

steps on the sapphire substrate is less likely to cause the changes in the epitaxial orientation of MoS_2.

The observed epitaxial relationship (0° domain) is in good agreement with those reported in Refs. 1, 8–11. and is the orthogonal configuration of those (90° domains) reported in Refs. 2–7. In addition, as shown in Figs. 6(a)-C and 6(b)-C, the 90° domains were not formed even when the sapphire substrate with the miscut orientation towards the [11$\bar{2}$0] direction was used, in marked contrast with the result in Ref. 3. We performed DFT calculations for the 0° and 90° domains to check if the formation of the 0° domain is governed by energetic stability, and found that the 0° domain is more stable by 0.164 eV/MoS_2(1 × 1). When the MoS_2 lattice is rotated by 90°, MoS_2 (5 × 5) is nearly lattice matched to Al_2O_3 ($2\sqrt{3} \times 2\sqrt{3}$)-R30°, resulting in a lattice mismatch of −4.18% (see Fig. S4 in the supplementary material). Thus, one may ascribe the higher stability of the 0° domain to smaller lattice mismatch (−0.42%). However, in actual systems, the formation of highly strained MoS_2 lattices is unlikely, because of weak van der Waals interaction between MoS_2 and Al_2O_3. Indeed, under the first-order approximation, the 90° domain becomes most stable in an incommensurate situation.[1] Thus, no definitive answer is available for the relative stability of the 0° and 90° domains on the basis of the DFT calculations.

In reviewing previous papers on the epitaxial relationship for MoS_2/sapphire, we found that the epitaxial orientation strongly depends on the growth method: the epitaxial relationship of MoS_2 [11$\bar{2}$0] // sapphire [11$\bar{2}$0] (0° domain) has been commonly observed for the MoS_2 ML grown by MOCVD,[8–11] while the growth using powder-source CVD results in the formation of 90° domains,[2–7] except for the result in Ref. 1. Thus, while not conclusive, it is possible that the two growth methods provide different growth environments, e.g., surface reconstructions, chemical adsorbates, and possible existence of interface layers, giving rise to the different epitaxial orientations of MoS_2.

V. CONCLUSIONS

We have studied the epitaxial relationship of MOCVD-grown MoS_2 on sapphire. LEED *I*–*V* curve analysis clearly shows that the MoS_2 ML is unidirectionally aligned with the sapphire substrate with the MoS_2 [11$\bar{2}$0] and [1$\bar{1}$00] directions being aligned with the Al_2O_3 [11$\bar{2}$0] and [1$\bar{1}$00] directions, respectively. On the basis of DFT calculations, we proposed the possible interface structures for MoS_2/sapphire, which agree well with the LEED experiments. The observed epitaxial relationship is hardly affected by the presence of surface steps on the sapphire substrate.

SUPPLEMENTARY MATERIAL

See the supplementary material for AFM images (Fig. S1) and Raman spectra (Fig. S2) for ML-MoS_2 on sapphire, XRD data for sapphire substrate with different off-directions (Fig. S3), and the atomic configurations of MoS_2 on sapphire for 0° and 90° domains (Fig. S4).

ACKNOWLEDGMENTS

We would like to thank T. Hiroto for XRD measurements. Theoretical calculations were performed by using the Numerical Materials Simulator of NIMS and the Earth Simulator (ES) of JAMSTEC. This work was partly supported by JST-CREST (Grant No. JPMJCR24A3) and JSPS KAKENHI (Grant No. JP23K04592).

AUTHOR DECLARATIONS

Conflict of Interest

The authors have no conflicts to disclose.

Author Contributions

Akihiro Ohtake: Conceptualization (equal); Data curation (lead); Formal analysis (lead); Investigation (equal); Methodology (lead); Writing – original draft (lead); Writing – review & editing (lead). **Jun Nara:** Conceptualization (equal); Data curation (lead); Formal analysis (lead); Investigation (equal). **Yoshiki Sakuma:** Conceptualization (lead); Funding acquisition (lead); Investigation (equal); Project administration (lead); Supervision (lead).

DATA AVAILABILITY

The data that support the findings of this study are available from the corresponding author upon reasonable request.

REFERENCES

[1]D. Dumcenco *et al.*, "Large-area epitaxial monolayer MoS_2," ACS Nano **9**, 4611–4620 (2015).
[2]A. Aljarb, Z. Cao, H.-L. Tang, J.-K. Huang, M. Li, W. Hu, L. Cavallo, and L.-J. Li, "Substrate lattice-guided seed formation controls the orientation of 2D transition-metal dichalcogenides," ACS Nano **11**, 9215–9222 (2017).
[3]T. Li *et al.*, "Epitaxial growth of wafer-scale molybdenum disulfide semiconductor single crystals on sapphire," Nat. Nanotechnol. **16**, 1201–1207 (2021).
[4]J. H. Fu *et al.*, "Oriented lateral growth of two-dimensional materials on c-plane sapphire," Nat. Nanotechnol. **18**, 1289–1294 (2023).
[5]L. Li *et al.*, "Epitaxy of wafer-scale single-crystal MoS_2 monolayer via buffer layer control," Nat. Commun. **15**, 1825 (2024).
[6]Y. Hua *et al.*, "Eight in. wafer-scale epitaxial monolayer MoS_2," Adv. Mater. **36**, 2402855 (2024).
[7]H. Chen, C. Ji, Y. Chen, H. Hou, W. Li, J. Shen, C. Cao, H. Zhu, H. Li, and W. Kong, "Interfacial atomic mechanisms of single-crystalline MoS_2 epitaxy on sapphire," Adv. Mater. **37**, 2414317 (2025).
[8]X. Xiang *et al.*, "Monolayer MoS_2 on sapphire: An azimuthal reflection high-energy electron diffraction perspective," 2D Mater. **8**, 025003 (2021).
[9]I. Kandybka, B. Groven, H. Medina Silva, S. Sergeant, A. Nalin Mehta, S. Koylan, Y. Shi, S. Banerjee, P. Morin, and A. Delabie, "Chemical vapor deposition of a single-crystalline MoS_2 monolayer through anisotropic 2D crystal growth on stepped sapphire surface," ACS Nano **18**, 3173–3186 (2024).
[10]C. Chen *et al.*, "Effect of growth temperature on the microstructure and properties of epitaxial MoS_2 monolayers grown by metalorganic chemical vapor deposition," J. Vac. Sci. Technol., A **42**, 022201 (2024).
[11]Y. Sakuma *et al.*, "Self-aligned and self-limiting van der Waals epitaxy of monolayer MoS_2 to annihilate grain boundaries for scalable 2D electronics," (unpublished), available at https://doi.org/10.21203/rs.3.rs-7386422/v1 (2025).
[12]J. Dong, D. Ding, C. Jin, Y. Liu, and F. Ding, "Edge reconstruction-dependent growth kinetics of MoS_2," ACS Nano **17**, 127–136 (2023).
[13]T. Yamasaki, A. Kuroda, T. Kato, J. Nara, J. Koga, T. Uda, K. Minami, and T. Ohno, "Multi-axis decomposition of density functional program for strong scaling up to 82 944 nodes on the K computer: Compactly folded 3D-FFT communicators in the 6D torus network," Comput. Phys. Commun. **244**, 264–276 (2019).
[14]W. Kohn and L. J. Sham, "Self-consistent equations including exchange and correlation effects," Phys. Rev. **140**, A1133–A1138 (1965).
[15]N. Troullier and J. L. Martins, "Efficient pseudopotentials for plane-wave calculations," Phys. Rev. B **43**, 1993–2006 (1991).
[16]D. Vanderbilt, "Soft self-consistent pseudopotentials in a generalized eigenvalue formalism," Phys. Rev. B **41**, 7892–7895 (1990).
[17]J. P. Perdew, K. Burke, and M. Ernzerhof, "Generalized gradient approximation made simple," Phys. Rev. Lett. **77**, 3865–3868 (1996).
[18]S. Grimme, "Semiempirical GGA-type density functional constructed with a long-range dispersion correction," J. Comput. Chem. **27**, 1787–1799 (2006).
[19]P. J. Rous, J. B. Pendry, D. K. Saldin, K. Heinz, K. Müller, and N. Bickel, "Tensor LEED: A technique for high-speed surface-structure determination," Phys. Rev. Lett. **57**, 2951–2954 (1986).
[20]P. J. Rous and J. B. Pendry, "The theory of tensor LEED," Surf. Sci. **219**, 355–372 (1989).
[21]J. B. Pendry, "Reliability factors for LEED calculations," J. Phys. C **13**, 937–944 (1980).
[22]T. J. Godin and J. P. LaFemina, "Atomic and electronic structure of the corundum (α-alumina) (0001) surface," Phys. Rev. B **49**, 7691–7696 (1994).
[23]X.-G. Wang, A. Chaka, and M. Scheffler, "Effect of the environment on α-Al_2O_3 (0001) surface structures," Phys. Rev. Lett. **84**, 3650–3653 (2000).
[24]J. Ahn and J. W. Rabalais, "Composition and structure of the Al_2O_3{0001}-(1 × 1) surface," Surf. Sci. **388**, 121–131 (1997).
[25]E. A. Soares, M. A. Van Hove, C. F. Walters, and F. F. McCarty, "Structure of the α-Al_2O_3 (0001) surface from low-energy electron diffraction: Al-termination and evidence for anomalously large thermal vibration," Phys. Rev. B **65**, 195405 (2002).